Article

Investigations on Physico-Mechanical and Spectral Studies of Zn^{2+} Doped P$_2$O$_5$-Based Bioglass System

M. Mohan Babu [1], P. Syam Prasad [1,*], S. Hima Bindu [1], A. Prasad [1], P. Venkateswara Rao [2], Nibu Putenpurayil Govindan [3], N. Veeraiah [4] and Mutlu Özcan [5]

[1] Department of Physics, National Institute of Technology Warangal, Warangal, Telangana 506004, India; mmbabu771@gmail.com (M.M.B.); h.bindu05@gmail.com (S.H.B.); prasadbabunitw@gmail.com (A.P.)

[2] Department of Physics, The University of the West Indies, Mona Campus, Kingston 7, Jamaica; pvrao54@gmail.com

[3] Joint Glass Centre of the IIC SAS, TnUAD and FChFT, Funglass, Alexander Dubček University of Trenčín, 91101 Trenčín, Slovakia; nibupg1@gmail.com

[4] Department of Physics, Acharya Nagarjuna University, Nagarjuna Nagar, Guntur 522510, India; profnvr@gmail.com

[5] Center for Dental and Oral Medicine, Division of Dental Biomaterials, Clinic for Reconstructive Dentistry, University of Zurich, 8006 Zurich, Switzerland; mutluozcan@hotmail.com

* Correspondence: syam9405@gmail.com or syamprasad@nitw.ac.in; Tel.: +91-833-296-9472

Abstract: ZnO incorporated phosphate based bioglasses with the composition xZnO–22Na$_2$O–24CaO–(54-X)P$_2$O$_5$ (where X = 2, 4, 6, 8, 10 mol%) were developed by melt-quenching process. The physical, thermal and other structural properties of the glasses were studied in detail. By employing various characterization techniques such as X-ray powder diffraction (XRD), Fourier transform infrared spectroscopy (FTIR), Scanning electron microscopy (SEM) in addition to the energy dispersion spectroscopy (EDS), and Raman spectroscopy, the structural properties were analyzed. Interestingly, physical, thermal and mechanical properties were enhanced with the increasing content of zinc oxide up to 8 mol%, due to the presence of more ionic nature of P–O–Zn bonds than P–O–P bonds in the glass network. The FTIR and Raman analysis revealed the evolution of the phosphate network with increasing zinc concentration and leads to progressive depolymerisation of the glass network. The obtained results from the physical and structural properties of these zinc added calcium phosphate glasses support their potential to use as bone implant applications.

Keywords: zinc oxide; P$_2$O$_5$-bioglass; glass-forming ability; structural properties; thermal stability

1. Introduction:

The phosphate based glass and glass ceramics are the most prominent materials in the repair and regeneration of damaged soft and hard tissues. In the 1970s Larry Hench and his co-workers developed a bioactive glass composition (45S5) successfully [1]. Several clinically approved bioactive glasses such as 45S5, 58S, and some silica based glasses are used excellently for bone and dental applications [2,3]. However, the long-term interaction of silica locally and systemically is not yet understood completely and raises the issue of the continuing reaction in vivo [4,5]. Due to accomplished bioactivity and substantiated biocompatibility, the bioactive glass-ceramics are used as promising materials for medical applications, especially in dental and orthopedic implants [6]. As an alternative to rarely absorb SiO$_2$ based glasses for tissue repair, P$_2$O$_5$ based glasses were developed by many researchers owing to specific properties such as higher values in biocompatibility, degradability, electrical conductivity and thermal expansion coefficient, with lower values in dissipation temperature, transition temperature and chemical durability [7,8]. Glasses made of phosphate have feasible applications in biology, batteries,

laser technologies, etc. [9]. The basic building blocks of crystalline and amorphous phosphates are the P-tetrahedra (PO4), which are formed via the covalent extrapolating of oxygen atoms and with the various phosphate anions; also, the structure of phosphate glass composition depends on the O/P ratio [10–12]. Among phosphate-based glasses, the calcium containing phosphate glasses possess high bioactivity. Moreover, these glasses are the best sites for bone bonding due to the chemical composition which is very close to the natural bone phase [13]. In general, phosphate-based glasses have high dissolution and poor chemical durability when compared with silicate and borate based glasses, which limits the applications. The control over degradation rate and improvement of chemical durability can be obtained by adding intermediate network modifiers such as transition metal oxides (Ca^{2+}, Na^+, Zn^{2+}, Mg^{2+}, Sr^{2+} and K^+) [14,15]. A highly explicable material is easily diminished through submissive dissolution in body fluids, impeding onset of the tissue remodeling method; a method of blending bioactive glass accompanied by other formidable and stabilized materials rather than sol-gel, the melt-derived bioactive glasses are more flexible [2]. Zinc is one of the most abundant trace elements present in bone and it shows a stimulatory effect on the formation of bone mineral phase in vitro and in vivo. In particular, zinc enhances quite well the bioglass chemical durability in aqueous solutions such as body fluids, and also moderately increases the mechanical strength [7,16,17]. Abou Neel et al. reported that the formation of bone bonding improves by replacing some content of calcium with zinc in bioglass system [7,18]. The glass modifier oxides such as Na_2O and CaO which are mixed with phosphate network control the extent of bioglass solubility in physiological environment [19]. In the recent past, Calcium phosphate based bioactive quaternary glass systems P_2O_5–CaO–Na_2O–K_2O were prepared by melt growth technique. Glasses were prepared in five different compositions by fixing P_2O_5 at 47 mol% and CaO at 30.5 mol% and by varying the K_2O and Na_2O concentrations [20]. The ability of the assembling bond and the physiological environment attributed to the ionic interaction with the host medium entrenched the bioactivity of the substance [21].

In this present article, we have reported the development of a novel ZnO–Na_2O–CaO–P_2O_5 bioglass system and the detailed investigations have been done to explore the effect of ZnO appropriateness for bone integrate implants.

2. Experimental Methods and Materials

2.1. Synthesis of Bioglass Samples

A high purity (99.9%) of chemicals P_2O_5, ZnO, CaO and Na_2O from Sigma-Aldrich (St. Louis, MO, USA) were used to synthesize the glass samples with the help of accustomed melt-quenching technique. The above mentioned chemicals were weighed in terms of batches and thoroughly blended in an agate mortar and then melted using a platinum crucible in the temperature range of 1000 °C for 2h. The homogeneous mixture of liquid melt was cast into pre-heated brass mould of pre-requisite dimensions and then transferred into an annealing furnace maintained at a temperature of 250 °C, below the glass transition temperature T_g for 2h and later on allowing them to cool slowly till room temperature for the removal of residual stress. The final form of glass samples were collected and used for various characterization purposes. The chosen glass composition and glass codes are shown in Table 1.

Table 1. Glass sample code and nominal glass composition details.

Glass Code	ZnO	Na₂O	CaO	P₂O₅
Z2	2	22	24	52
Z4	4	22	24	50
Z6	6	22	24	48
Z8	8	22	24	46
Z10	10	22	24	44

2.2. Physical Parameters and Microhardness

2.2.1. Physical Parameters

A digital balance of model BSA22S-CW: Sartorius with a certainty of ±0.0001g was used to measure the densities of the prepared bioglass samples. The density calculations were done by applying the Archimedes principle with O-xylene as a buoyant liquid. The standard formula used for density measurement is:

$$\rho_g = \frac{Wa}{Wa - Wxylene} \times \rho_{xylene} \tag{1}$$

where Wa = weight in air, W_{Xylene} = weight in xylene and ρ_{xylene} = density of xylene (0.867 g/cm^3).

In order to get accuracy in density, the average value of five replicates was considered in calculations. Further crucial substantial physical parameters, Oxygen molar volume (V_O), Molar volume (V_m) and Oxygen packing density (OPD) were deliberated with precision utilizing density and standard formulas $V_O = (\sum x_i M_i / \rho_g)(1/\sum x_i n_i)$, $V_m = \sum x_i M_i / \rho_g$ and OPD = 1000C (ρ/M), respectively [22,23]. Where C = number of oxygen atoms per each configuration, x_i = molar fraction of each component, M = molecular weight of bioglass, ρ_g = glass density, n_i = number of oxygen atoms in each oxide and M_i = molecular weight of each component.

2.2.2. Microhardness and Fracture Toughness

The SHIMADZU-HMV-G20S (Shimadzu, Kyoto, Japan), microhardness tester was employed in the microhardness (Hv) test of the prepared samples, at an ambient temperature under a weight of 1.96 N and a retention period of 15s applied. For certainty of the measurement, ten indentations were taken at different points on the surface of each specific sample. The consequential traces of the indentations were captured and after unloading the corresponding length of the indentation imprint diagonals and the length of the crashes originated from the corners of the indentation imprints were also recorded by a high resolution microscope. These indentation measurements were carried out at ambient temperature with relative humidity. The fracture toughness (K_{IC}) and microhardness (Hv) were calibrated with the help of the formula:

$$H_v = 1.854 \frac{F}{d^2} \tag{2}$$

where H_v = Vickers hardness in GPa, F = applied force in newton and d = mean length of the diagonals of the indentation in meters. The following formula is used for K_{IC} the glass fracture toughness:

$$K_{IC} = 0.016 \, H_v \frac{a^2}{C^{3/2}} \tag{3}$$

and units is in (MPa m$^{1/2}$), where a = half-length of diagonal of indentation, c = crack length of the center of indentation to the crash end [24].

2.3. Thermal Properties

With the help of the NETZSCH-STA 2500 (NETZSCH, Selb, Germany) Regulus thermal analysis system, DTA & TG measurements were carried out on glass powder samples in an air medium from room temperature to 1000 °C with a heating frequency of 10 K min^{-1}. The glass powders with ~20 mg quantity were taken in an alumina crucible and powdered alumina was used as a reference material to determine the crystallization temperature (Tc), melting temperatures (Tm) and glass transition temperature (Tg). The difference between Tc and Tg representing the thermal stability (ΔT) and the ration between Tc − Tg and Tm − Tc gives Hruby's criterion (H) of the glass system:

$$\Delta T = Tc - Tg \tag{4}$$

and

$$H = \frac{Tc - Tg}{Tm - Tc} \tag{5}$$

2.4. Structural Description of Bioglasses

A PANalytical X'pert Powder (Malvern Panalytical Ltd, Malvern, UK), XRD is using Cu–Kα as a radiation source was used to confirm the amorphous nature of the prepared bio-glass samples at a diffraction angle scanning in the range of 10°–80° with a step scope resolution of 0.001° and 20 s time per step. FTIR (PerkinElmer, Shelton, USA) transmittance spectroscopy (model: S100, PerkinElmer) was employed in the wavenumber region between 400–4000 cm^{-1} for the functional group analysis. The bioglass samples were blended carefully with KBr powder, and then sent for pressing to form pellets under vacuum pressure for analyzing the functional groups present in the prepared samples. The Raman spectra of zinc incorporated P$_2$O$_5$ bioglass were performed using a Renishaw Invia Reflex Micro Raman Spectrometer (Renishaw plc, Wootton-under-Edge, UK) in the range of 100–1800 cm^{-1} at the room temperature and using an Argon ion laser of excitation 514.5 nm under backscattering alignment. The FTIR and Raman spectra were deconvoluted (With Lorenz-type function by using an Origin 8.5 software), in order to get the information on the various structural bands present in the prepared glasses [25]. The morphology and microstructure of the bioglass samples were characterized by using a SEM of VEGA 3 LMU, TESCAN (TESCAN, Brno–Kohoutovice, Czech Republic) [23].

3. Results and Discussion

3.1. Physical Parameters of the Bioglasses

The experimental results of various physical parameters like oxygen packing density (OPD), oxygen molar volume (V$_O$), molar volume (V$_m$), and density (ρ_g) of the bioglasses are summarized in Table 2. The ZnO concentration (in mol%) versus density, oxygen packing density, oxygen molar volume and molar volume are shown in Figure 1a,b. The physical parameters V$_O$ and ρ_g were found to be increasing, whereas the OPD and Vm tended to be decreased with the increase in ZnO concentration. The Vo of the prepared samples exhibited a slight increase from 24.143 to 24.504 cm^3/mol. The increase in density clearly indicates the presence of more ionic nature of P–O–Zn bonds than P–O–P bonds in the glass network, produces the compactness of the glass structure [26] and also due to the higher density of ZnO (5.61 g cm^{-3}) when compared to P$_2$O$_5$ (2.30 g cm^{-3}) [27]. Conversely, the decrease in molar volume was a result of depletion in the mole fraction of the oxygen ions in the glass sample [28]. The diminishing of molar volume can be ascribed to the strong bond strength of Zn–O bond in comparison to P–O–P and P–O bonds which results in smaller bond lengths consequently causing a tightening of the glass network [27,29,30]. The replacement of P$_2$O$_5$ by ZnO is the primary cause of systematic decreases as the ionic radii of oxygen ions are higher when compared with radii of both the Zn and P ions [31,32]. Oxygen packing density (OPD) of the glasses varied from 76.389 to 72.667 mol/L and were found to decrease with the content of Zinc oxide (2 to 10 mol%) which is attributing to the less tightly packing of oxygen atoms in the glass network [22].

Table 2. Physical parameters of the ZnO–Na$_2$O–CaO–P$_2$O$_5$ glass system.

Sample Code	Molar Mass (g/mol)	Molar Volume (Vm) (cm^3/mol)	Density (ρ_g) (g/cm^3)	Oxygen Molar Volume (Vo) (cm^3/mol)	Oxygen Packing Density (OPD) (mol/L)	Vickers Hardness Hv (GPa)	Fracture Toughness, K$_{IC}$ (MPa m$^{1/2}$)
Z2	102.532	40.319 (±0.626)	2.543 (±0.068)	24.143 (±1.207)	76.389 (±1.785)	2.615 (±0.074)	0.176 (±0.004)
Z4	101.321	39.765 (±0.757)	2.548 (±0.077)	24.247 (±1.514)	75.443 (±1.782)	2.652 (±0.075)	0.183 (±0.005)
Z6	100.110	39.151 (±0.672)	2.557 (±0.072)	24.317 (±1.424)	74.582 (±1.981)	2.763 (±0.097)	0.198 (±0.004)
Z8	98.898	38.497 (±0.589)	2.569 (±0.069)	24.365 (±1.142)	73.772 (±1.528)	3.190 (±0.092)	0.250 (±0.005)
Z10	97.687	37.981 (±0.676)	2.572 (±0.076)	24.504 (±1.332)	72.667 (±1.762)	2.781 (±0.100)	0.196 (±0.004)
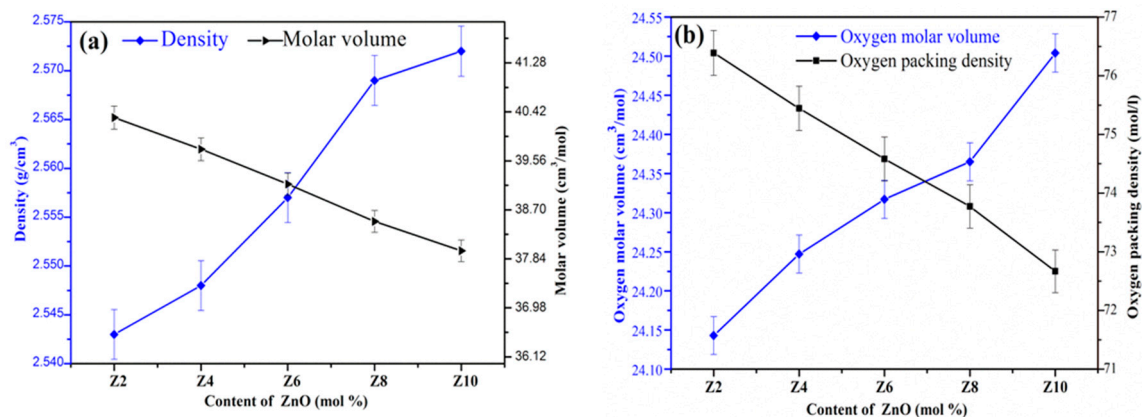
Figure 1. Variability of distinct physical parameters of glasses investigation with the increase in content of ZnO (mol%): (**a**) Density (g/cm^3) and molar volume (**b**) Oxygen packing density and Oxygen molar volume.

3.2. Thermo Gravimetric-Differential Thermal Analysis

The perusal of various thermal parameters such as Hruby's criterion (H), crystallization temperature (Tc), transition temperature (Tg), thermal stability (ΔT) and melting temperature (Tm) of the glass system is essential to understand the structural transformations with different temperatures. From DTA traces the upward peaks indicate that Tc and Tg are due to exothermic reaction and the downward peak indicates Tm is characterized by endothermic reactions. The different thermal parameters are labeled in Table 3, and DTA traces are displayed in Figure 2a. The glass transition (Tg) values (343.31–348.52 °C) increased with the increase in ZnO up to 8 mol% and then declines in higher concentration of ZnO. While in the case of crystallization temperature (Tc) (458.73–469.12 °C) and melting temperature (Tm) (716.18–699.75 °C), a general decrease in trend was found with the increase of ZnO. Tg increased with an increase of ZnO from 2 mol% to 8 mol% was due to enhancement in the average cross link density through non bridging oxygen ions (NBO) and the number of bonds per unit volume. In addition, the increase in Tg can also be imputable to the expanding cumulative sequel of ZnO on glass network and deliberate movement of huge Zn^{2+} ions, leading to more rigidity of the glass network [29,30]. Further increasing the ZnO concentration led to the slight decrease in Tg from 348.52 °C to 344.3 °C, which is owing to the intrusion of P–O–P bonds on account of Zn^{2+} ions [29]. It is attributed to the high amount of depolymerization in the glass matrix [33]. The thermal stability (ΔT) is the measure of the glass network and rigidity, whereas Hruby criterion (H) gives the glass-forming tendency of the chosen materials. In the present ZnO doped glasses, the values of stability (ΔT) increased from 111.26 °C to 121.19 °C and Hruby criterion (H) increased from 0.4483 to 0.5154, clearly indicating the high strength and good glass-forming trend of all glasses. The greater the value of (ΔT) and smaller the difference of Tm−Tc will decelerate the crystallization against devitrification of the

glass network, which leads the glass formation [30]. In the present system, Z8 is conformed as the best glass because of its high thermal stability (ΔT) and Hruby criterion (H) values.

Table 3. Thermal properties of ZnO doped phosphate bioactive glasses.

Sample code	Tg (°C)	Tc (°C)	Tm (°C)	ΔT (°C)	K_H
Z2	343.31 (±0.343)	458.73	716.18	115.42 (±1.154)	0.4483
Z4	345.27 (±0.346)	456.53	714.11	111.26 (±1.112)	0.4319
Z6	346.89 (±0.347)	459.12	709.86	112.23 (±1.122)	0.4475
Z8	348.52 (±0.349)	469.12	704.43	121.19 (±1.211)	0.5154
Z10	344.63 (±0.344)	458.98	699.75	114.35 (±1.143)	0.4749
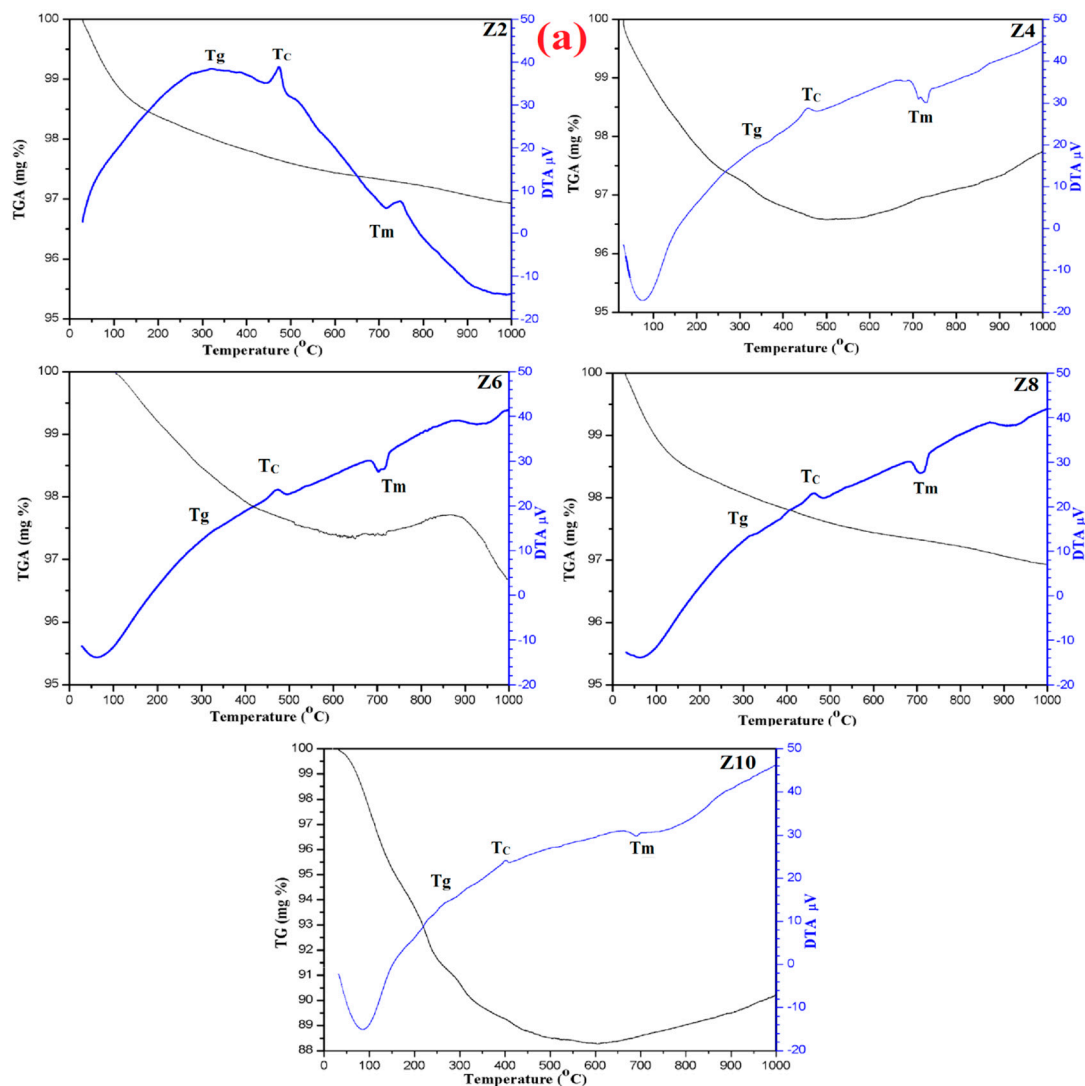
Figure 2. *Cont.*
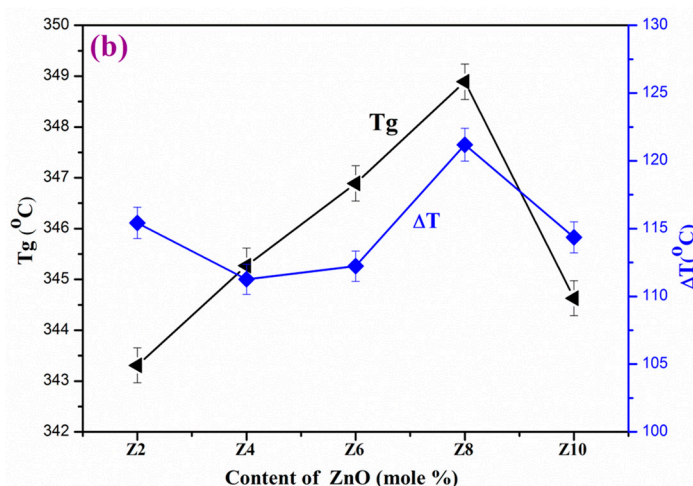
Figure 2. (**a**) TG-DTA traces of Z2, Z4, Z6, Z8 and Z10 bioglasses and (**b**) variation of thermal stability and glass transition (Tg) as a function of ZnO (mol%).

A significantly slight weight loss was observed at two regions of the TG curves shown in the Figure 2b along with DTA traces. The first weight loss of ~1.59% of Z2 sample appeared from the room temperature to ~128 °C and the second weight loss was around ~2.64%, from the temperature between ~128 °C to ~626 °C. In the Z4 sample the first weight loss of ~1.93% found from room temperature to 166 °C and the second weight loss was ~3.25% from the 166 °C to 449 °C. The TG curve of Z6 sample was observed from ambient temperature to 325 °C with a first weight loss of ~2.42% and a second weight loss of 3.18% from 325 °C to 623 °C. Similarly, for Z8 and Z10 the first weight loss of ~1.35% (from room temperature to 120 °C) and ~5.21% (room temperature to 159 °C), respectively. The second weight loss of ~2.51% from 120 °C to 610 °C and ~9.59% from 159 °C to 340 °C of samples Z8 and Z10, respectively. The first stage of weight loss at around 76 °C to 250 °C was due to the loss of hydrated and coordinated water molecules, which came into the ambient environment and the second stage of weight loss at around 300 °C to 600 °C is attributed to residual precursor phosphorus from the glass composition. After this, there was no considerable weight loss noticed with a rise in temperature up to 1000 °C. The low loss of weight indicates the high rigidity of the glass network of as-developed samples [32].

3.3. Vickers Hardness and Fracture Toughness

The mechanical properties, in particular fracture toughness and hardness, are very essential for any material to know the structural compactness. Calcium phosphate glasses gain reasonably better improvement in mechanical properties with the addition of ZnO. The discrepancy of fracture toughness and Vickers microhardness as a function of the ZnO content of the prepared bioglasses system are shown in Figure 3a,b, and the associated values are tabulated in Table 2. It is observed that fracture toughness and Vickers microhardness values progressively increase from 2.615 (±0.0742) GPa to 3.190 (±0.0921) GPa and from 0.17609 (MPa m$^{1/2}$) to 0.25099 (MPa m$^{1/2}$), respectively, with the increase in ZnO content in the glass matrix. Figure 3c shows the optical microscopic Vickers indent impressions for Z2, Z4 and Z8 glasses. The prepared bio-glass samples fracture toughness was being measured with the help of crack length and Hv values from Vickers indent impressions of the samples using the optical microscope. A gradual rise in the obtained toughness and microhardness values of the bioglasses, with increasing ZnO content was on account of the expansion of the glass network in accordance with the increase in inter-atomic spacing or bond length between the atoms. Zn^{2+} ions enter interstitially in the glass network to form more P–O–Zn linkages by decaying the P–O–P bonds. Consecutively, it brings down the number of non-bridging oxygens (NBO's) and enhances the rigidity, compactness and cross-linking density of the glass network [34]. In the present as-prepared glasses, Z8 has highest Hv and K$_{IC}$ values. It was found that there was an increase in hardness and the toughness from Z2

(2 mol%) to Z8 (8 mol%), and then decreases slightly for Z10 (10 mol%), which was apparently due to the decrease in packing density [35,36]. It means there was breaking of some P–O–Zn bonds per volume in the glass network during the application of load, which led to a decrease in the resistance of deformation.
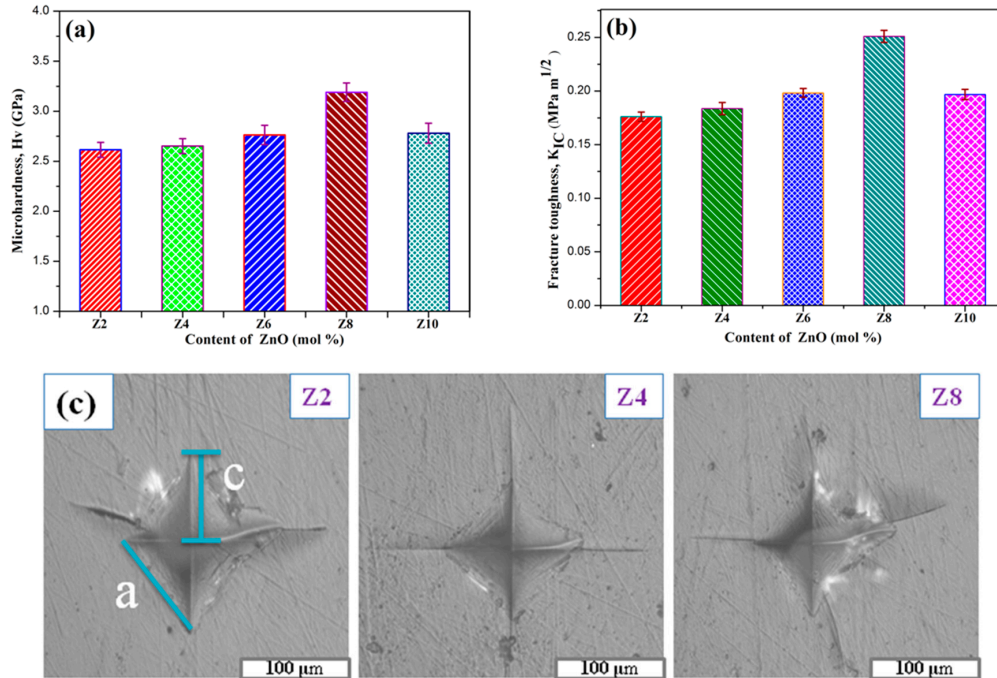

Figure 3. (**a**) Microhardness and (**b**) fracture toughness of the Z2, Z4, Z6, Z8 and Z10 glasses as a function of the ZnO (mol%) and (**c**) Optical images of Vickers Indentation from Z2, Z4 and Z8 glass samples.

3.4. XRD Analysis

The XRD results of all prepared bioglass specimens (Z2, Z4, Z6, Z8 and Z10) are shown in Figure 4. The samples show a broad hump at around 25° indicating the lack of a long-range order in the structure and also confirm the amorphous nature of all bioglasses [37].
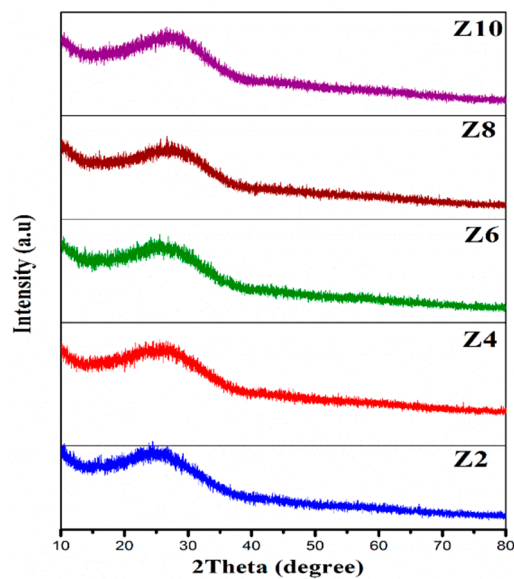

Figure 4. X-ray diffraction patterns of Z2, Z4, Z6, Z8 and Z10 glasses.

3.5. SEM-EDS Micrographs Analysis

Figure 5 shows the EDS spectra and SEM micrographs of zinc incorporated bio glasses surfaces, respectively. The EDS spectrum demonstrates the presence of Ca, P, Na, O and Zn elements in the glass samples and the appearance of smooth, compact and plane surface morphology from the SEM micrographs confirmed no morphological changes in the prepared glasses.
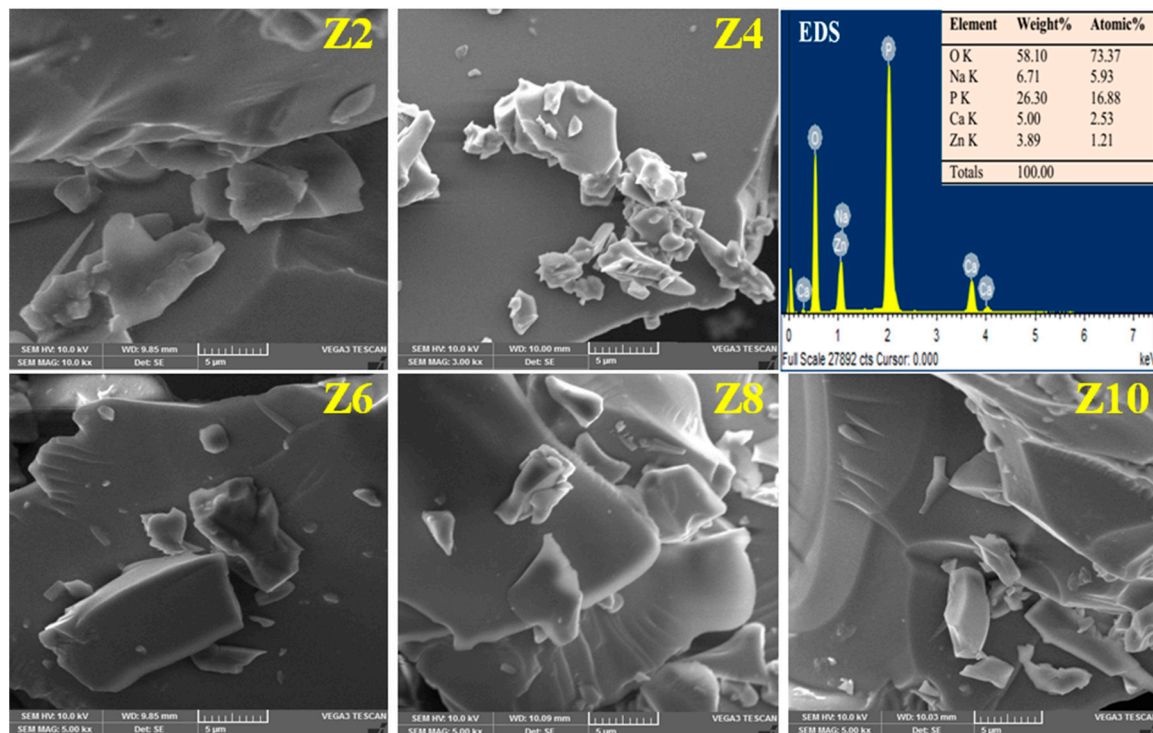

Figure 5. SEM micrographs and EDS spectra of ZnO doped phosphate bioglass samples.

3.6. FTIR Spectroscopic Analysis

Figure 6 shows the FTIR spectroscopic pattern of the bioglass samples Z2, Z4, Z6, Z8 and Z10 presents some intense absorption bands at 526, 720, 900, 1105 and 1270 cm^{-1} and weak absorption at 1643, 2382 cm^{-1} and broad band of absorption peak around 3470 cm^{-1}. These bands are the evidence of the existence of phosphate groups in the glass network.

A detailed investigation on the structural changes in glasses (shown here for Z2 glass only) has been identified by using the deconvoluted FTIR spectra (Figure 7). From the FTIR spectra, the bioglass samples consist of an absorption band at around 485 cm^{-1} that are ascribed to the presence of Zn–O vibrations of ZnO_4 structural units [38]. The absorption band at around 526 cm^{-1} perhaps designed by the consonance of P–O–P bending vibration and also due to the distortion mode of PO^- groups (deformation mode of P–O^- and (PO_4^{3-}) groups) [28,29,33,39]. The peaks positioned at 720 cm^{-1} and 770 cm^{-1} are due to both asymmetric and symmetric stretching of P–O–P groups [40]. The appearance of bands at 886 cm^{-1} and 900 cm^{-1} are attributed to asymmetric stretching and symmetric stretching modes of P–O–P groups, respectively [26,39,41]. A peak at 996 cm^{-1} is noticed due to asymmetric stretching vibration of PO3 groups [41] and the band at 1105 cm^{-1} is observed due to vibrations of a phosphate group (P–O^-) or might be P–O–Zn linkages [7,17,42,43]. A little intense band at around ~1270 cm^{-1} was assigned due to the (O–P–O) bonds, which is the asymmetric stretching vibration of O–P–O bonds [41]. Nearly at around 1643 cm^{-1} a weak intense band is accredited because of the P–O–H bond. Such groups contribute to most strong hydrogen bonding with non-bridging oxygen [44]. At the range of 2382 cm^{-1} a weak band is observed due to the different structural sites as a stretching vibration of the P–O–H group or the stretching of CO_2 [27]. Strong absorption bands at around 3472 cm^{-1} and

a weak band at 3524 cm^{-1} are observed due to the existence of water molecules (corresponding to OH groups) in the glass matrix (Figure 7). The presence of water is probably due to the retention of atmospheric moisture by the phosphate glass sample or pellet, and resulting in the appearance of the H–O–H bond, belongs to water molecules; the present sample does not carry water as a unit in the glass network [45].
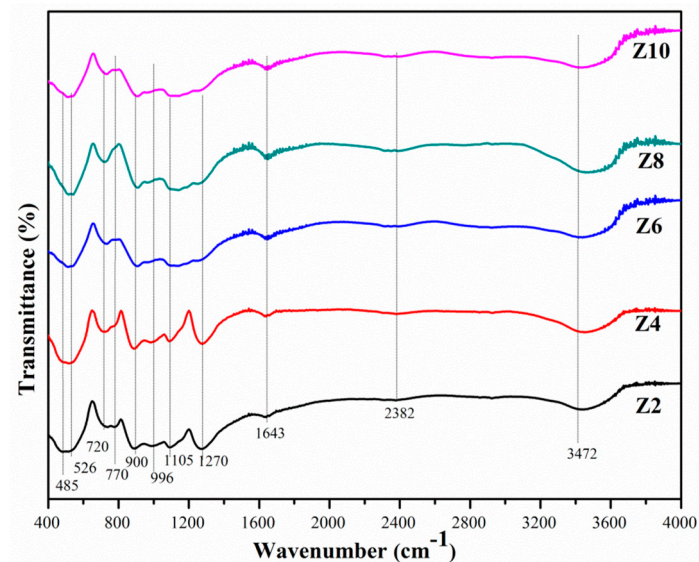

Figure 6. FTIR spectra of ZnO doped phosphate (Z2, Z4, Z6, Z8 and Z10) bioglasses.
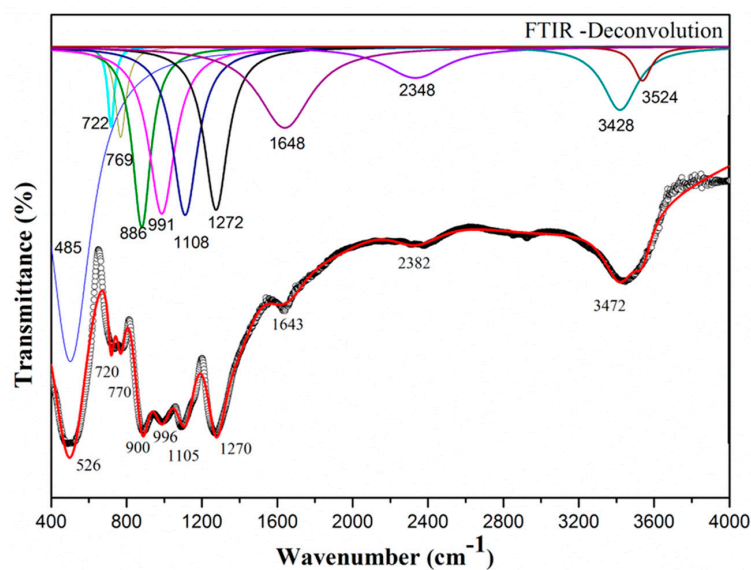
Figure 7. Deconvoluted FTIR spectra of the glass (Z2) and curve fit.

3.7. Raman Spectra

Raman spectroscopy is used to get the information of various functional groups of both inorganic and organic phases on the molecular level [37] which act as a powerful analytical technique for biomedical applications and is used to study the structure of many bioglass samples [46,47]. Figure 8 illustrates the Raman spectra of ZnO incorporated phosphate glasses. Deconvoluted Raman spectra (Figure 9) is also plotted for the identification of specific component bands for the developed glasses, but unfortunately no significant additional bands are observed after deconvoluted Raman spectra. From the obtained spectra, the ZnO doped phosphate bioglasses are exhibited four prominent bands at

318 cm^{-1}, 386 cm^{-1}, 666 cm^{-1}, 1168 cm^{-1}, and 1294 cm^{-1}. On the low frequency side a strong band at 318 cm^{-1} can be ascribed to the symmetric stretching vibrations in the $(PO_4)^{3-}$ tetrahedral chains [48] and a feeble band at 386 cm^{-1} is attributed to the bending motion of phosphate polyhedral [41]. The broad band at 666 cm^{-1} is attributed to symmetric stretching vibration of the spanning oxygen attaching two PO_4 tetrahedron (P–O–P) in phosphate chains [49]. The sharp band at 1168 cm^{-1} is ascribed to the symmetric stretching mode of O–P–O non-bridging oxygens, signifying the evolution of phosphate tetrahedral. From the bands at 1294 cm^{-1} can be referred to the symmetric stretch of the P=O terminal oxygens [48,50,51]. It is clearly observed that, with increasing concentration of ZnO mol% in the calcium phosphate glasses, there was a gradual decrement in the band intensities positioned at 1294, 1169, 666, 386 and 318 cm^{-1}, which was mainly due to the disruption of the vitreous phosphate network (P–O–P linkages) by ZnO and leading to the structure depolymerization and the formation of non-bridging oxygens (NBO) [25,26,33,43].
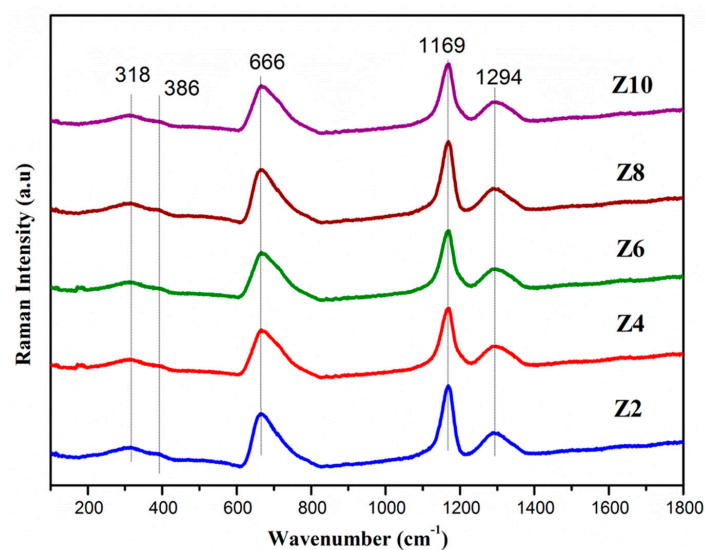

Figure 8. Raman spectra of Z2, Z4, Z6, Z8 and Z10 glasses at room temperature.
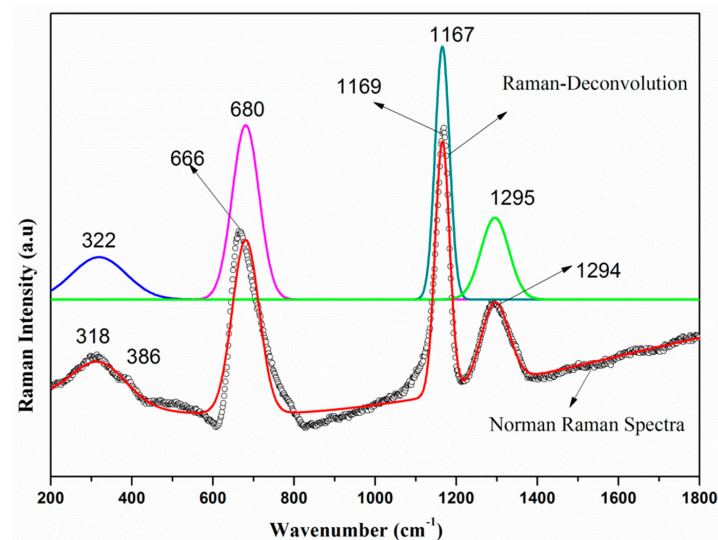

Figure 9. Deconvoluted Raman spectra of the glass (Z2) Sample.

Moreover, it is perceived that there was no significant variation in peak positions, indicating the geometric invariability of Q^2 units for zinc ion accumulation up to 10 mol% of ZnO [51]. Interestingly,

we observed that there is a good correlation between the Raman band intensities and the band intensities of FTIR spectra with the content of ZnO.

These small structural changes observed from FTIR and Raman spectra concluded the modifier role of ZnO by depolymerizing the phosphate chains with the addition of small quantities of ZnO in the phosphate glass network.

4. Conclusions

The present study researched enhanced structural and mechanical strength of ZnO incorporated P_2O_5 based bioglasses for biomedical applications. The physical parameters such as oxygen molar volume and the density were increases, whereas oxygen packing density and the molar volume tended to decline with the rise of ZnO concentration. The glass transition temperature (Tg) increased with the ZnO content up to 8 mol% and then decreased for 10 mol% of ZnO. The increase in Tg could be ascribed to enhance the aggregation effect of ZnO on the glass network and a deliberate moment of large Zn^{2+} ions, which result in rather high rigidity of the glass network. Vickers microhardness and toughness values of the as-prepared bioglasses increases, with increasing ZnO content is for expansion of the glass network in accordance with the rise in inter-atomic spacing or bond length between the atoms. Zn^{2+} ions entered interstitially in the glass network to form more P–O–Zn linkages by shattering the P–O–P bonds, consecutively, and reduced the number of non-bridging oxygens and intensifies the rigidity, compactness and cross-linking density of the glass network. In the present as-prepared glasses Z8 had the highest Hv and K_{IC} values. The amorphous nature and facade morphology of the glasses were confirmed by XRD and SEM analysis, respectively. The Raman spectra and FTIR indicates the progressive depolymerisation of glass network by the evolution of the phosphate network with an increasing zinc concentration. According to the above-mentioned final conclusions, it is noteworthy that, out of all glasses, Z8 (8 mol%) exhibited enhanced properties that might be used in the advancement of resorbable materials in the bone.

References

1. Hench, L.L.; Paschall, H.A. Direct chemical bond of bioactive glass-ceramic materials to bone and muscle. *J. Biomed. Mater. Res.* **1973**, *7*, 25–42. [CrossRef] [PubMed]
2. Hench, L.L. Bioceramics: From Concept to Clinic. *J. Am. Ceram. Soc.* **1991**, *74*, 1487–1510. [CrossRef]
3. Neel, E.A.A.; Knowles, J.C. Physical and biocompatibility studies of novel titanium dioxide doped phosphate-based glasses for bone tissue engineering applications. *J. Mater. Sci. Mater. Electron.* **2007**, *19*, 377–386. [CrossRef] [PubMed]
4. Skelton, K.; Glenn, J.; Clarke, S.A.; Georgiou, G.; Valappil, S.; Knowles, J.C.; Nazhat, S.; Jordan, G.R. Effect of ternary phosphate-based glass compositions on osteoblast and osteoblast-like proliferation, differentiation and death in vitro. *Acta Biomater.* **2007**, *3*, 563–572. [CrossRef] [PubMed]
5. Ahmed, I.; Lewis, M.; Olsen, I.; Knowles, J.C. Phosphate glasses for tissue engineering: Part 1. Processing and characterisation of a ternary-based P_2O_5-CaO-Na_2O glass system. *Biomaterials* **2004**, *25*, 491–499. [CrossRef]
6. Groh, D.; Döhler, F.; Brauer, D.S. Bioactive glasses with improved processing. Part 1. Thermal properties, ion release and apatite formation. *Acta Biomater.* **2014**, *10*, 4465–4473. [CrossRef]

7. Neel, E.A.A.; Pickup, D.M.; Valappil, S.P.; Newport, R.; Knowles, J.C. Bioactive functional materials: A perspective on phosphate-based glasses. *J. Mater. Chem.* **2009**, *19*, 690–701. [CrossRef]

8. Lu, M.; Wang, F.; Chen, K.; Dai, Y.; Liao, Q.; Zhu, H. The crystallization and structure features of barium-iron phosphate glasses. *Spectrochim. Acta Part A Mol. Biomol. Spectrosc.* **2015**, *148*, 1–6. [CrossRef]

9. Hejda, P.; Holubová, J.; Černošek, Z.; Cernosková, E. The structure and properties of vanadium zinc phosphate glasses. *J. Non-Cryst. Solids* **2017**, *462*, 65–71. [CrossRef]

10. Magdas, D.A.; Vedeanu, N.; Toloman, D. Study on the effect of vanadium oxide in calcium phosphate glasses by Raman, IR and UV–vis spectroscopy. *J. Non-Cryst. Solids* **2015**, *428*, 151–155. [CrossRef]

11. Hoppe, U.; Walter, G.; Kranold, R.; Stachel, D. Structural specifics of phosphate glasses probed by diffraction methods: A review. *J. Non-Cryst. Solids* **2000**, *263*, 29–47. [CrossRef]

12. Brow, R.K. Review: The structure of simple phosphate glasses. *J. Non-Cryst. Solids* **2000**, *263*, 1–28. [CrossRef]

13. Lucacel, R.C.; Maier, M.; Simon, V. Structural and in vitro characterization of TiO_2-CaO-P_2O_5 bioglasses. *J. Non-Cryst. Solids* **2010**, *356*, 2869–2874. [CrossRef]

14. Othman, H.A.; Arzumanyan, G.; Möncke, D. The influence of different alkaline earth oxides on the structural and optical properties of undoped, Ce-doped, Sm-doped, and Sm/Ce co-doped lithium alumino-phosphate glasses. *Opt. Mater.* **2016**, *62*, 689–696. [CrossRef]

15. Knowles, J.C. Phosphate based glasses for biomedical applications. *J. Mater. Chem.* **2003**, *13*, 2395. [CrossRef]

16. Wu, C.; Chang, J.; Zhai, W. A novel hardystonite bioceramic: Preparation and characteristics. *Ceram. Int.* **2005**, *31*, 27–31. [CrossRef]

17. Chajri, S.; Bouhazma, S.; Herradi, S.; Barkai, H.; Elabed, S.; Koraichi, S.I.; el Bali, B.; Lachkar, M. Studies on preparation and characterization of SiO_2–CaO–P_2O_5 and SiO_2–CaO–P_2O_5–Na_2O bioglasses subtituted with ZnO. *J. Mater. Environ. Sci.* **2016**, *7*, 1882–1897.

18. Ouis, M.A. Effect of ZnO on the Bioactivity of Hench's Derived Glasses and Corresponding Glass-Ceramic Derivatives. *Silicon* **2011**, *3*, 177–183. [CrossRef]

19. Carta, J.C.D.; Pickup, D.M.; Knowles, J.C.; Ahmed, I.; Smith, M.E.; Newport, R. A structural study of sol–gel and melt-quenched phosphate-based glasses. *J. Non. Cryst. Solid.* **2007**, *353*, 1759. [CrossRef]

20. Marikani, A.; Maheswaran, A.; Premanathan, M.; Amalraj, L. Synthesis and characterization of calcium phosphate based bioactive quaternary P_2O_5–CaO–Na_2O–K_2O glasses. *J. Non. Cryst. Solid.* **2008**, *354*, 3929–3934. [CrossRef]

21. Lunkenheimer, P.; Rall, H.; Alkemper, J.; Fuess, H.; Böhmer, R.; Loidl, A. Ionic motion in bioactive ceramics investigated by dielectric spectroscopy. *Solid State Ion.* **1995**, *81*, 129–134. [CrossRef]

22. Rao, V.H.; Prasad, P.S.; Rao, P.V.; Santos, L.F.; Veeraiah, N. Influence of Sb_2O_3 on tellurite based glasses for photonic applications. *J. Alloys Compd.* **2016**, *687*, 898–905. [CrossRef]

23. Babu, M.M.; Prasad, P.S.; Rao, P.V.; Govindan, N.P.; Singh, R.K.; Kim, H.-W.; Veeraiah, N. Titanium incorporated Zinc-Phosphate bioactive glasses for bone tissue repair and regeneration: Impact of Ti^{4+} on physico-mechanical and in vitro bioactivity. *Ceram. Int.* **2019**, *45*, 23715–23727. [CrossRef]

24. Abo-Naf, S.M.; Khalil, E.; El-Sayed, E.-S.M.; Zayed, H.A.; Youness, R.A. In vitro bioactivity evaluation, mechanical properties and microstructural characterization of Na_2O–CaO–B_2O_3–P_2O_5 glasses. *Spectrochim. Acta Part A Mol. Biomol. Spectrosc.* **2015**, *144*, 88–98. [CrossRef] [PubMed]

25. Stefanovsky, S.V.; Stefanovsky, O.; Kadyko, M.; Presniakov, I.; Myasoedov, B. The effect of Fe_2O_3 substitution for Al_2O_3 on the phase composition and structure of sodium–aluminum–iron phosphate glasses. *J. Non-Cryst. Solids* **2015**, *425*, 138–145. [CrossRef]

26. Omrani, R.O.; Krimi, S.; Videau, J.J.; Khattech, I.; El Jazouli, A.; Jemal, M. Structural and thermochemical study of Na_2O–ZnO–P_2O_5 glasses. *J. Non-Cryst. Solids* **2014**, *390*, 5–12. [CrossRef]

27. Kapoor, S.; Goel, A.; Correia, A.F.; Pascual, M.J.; Lee, H.-Y.; Kim, H.-W.; Ferreira, J.M.F. Influence of ZnO/MgO substitution on sintering, crystallisation, and bio-activity of alkali-free glass-ceramics. *Mater. Sci. Eng. C* **2015**, *53*, 252–261. [CrossRef]

28. Anigrahawati, P.; Sahar, M.; Ghoshal, S. Influence of Fe3O4 nanoparticles on structural, optical and magnetic properties of erbium doped zinc phosphate glass. *Mater. Chem. Phys.* **2015**, *155*, 155–161. [CrossRef]

29. Rajkumar, G.; Aravindan, S.; Rajendran, V. Structural analysis of zirconia-doped calcium phosphate glasses. *J. Non-Cryst. Solids* **2010**, *356*, 1432–1438. [CrossRef]

30. Zhang, L.; Liu, S. Structure and crystallization behavior of $50CuO$–$xTiO_2$–$(50-x)P_2O_5$ (x = 5–20) glasses. *J. Non-Cryst. Solids* **2017**, *473*, 108–113. [CrossRef]

31. Ahmed, K.F.; Ibrahim, S.O.; Sahar, M.R.; Mawlud, S.Q.; Khizir, H.A. Thermal analyses, spectral characterization and structural interpretation of Nd^{3+}/Er^{3+} ions co-doped TeO_2–$ZnCl_2$ glasses system. In *AIP Conference Proceedings*; AIP Publishing LLC: College Park, MD, USA, 2017.

32. Kalita, H.; Kumar, B.P.; Konar, S.; Tantubay, S.; Mahto, M.K.; Manda, M.; Pathak, A. Sonochemically synthesized biocompatible zirconium phosphate nanoparticles for pH sensitive drug delivery application. *Mater. Sci. Eng. C* **2016**, *60*, 84–91. [CrossRef] [PubMed]

33. Oueslati-Omrani, R.; Hamzaoui, A.H. Effect of ZnO incorporation on the structural, thermal and optical properties of phosphate based silicate glasses. *Mater. Chem. Phys.* **2020**, *242*, 122461. [CrossRef]

34. Amin Matori, K.; Mohd Zaid, M.H.; Quah, H.J.; Abdul Aziz, S.H.; Abdul Wahab, Z.; Mohd Ghazali, M.S. Studying the Effect of ZnO on Physical and Elastic Properties of $(ZnO)_x(P_2O_5)_{1-x}$ Glasses Using Nondestructive Ultrasonic Method. *Adv. Mater. Sci. Eng.* **2015**, *2015*, 596361. [CrossRef]

35. Januchta, K.; Youngman, R.E.; Goel, A.; Bauchy, M.; Rzoska, S.J.; Bockowski, M.; Smedskjaer, M.M. Structural origin of high crack resistance in sodium aluminoborate glasses. *J. Non-Cryst. Solids* **2017**, *460*, 54–65. [CrossRef]

36. Yuan, K.; Sun, Y.; Lu, Y.; Liang, X.; Tian, D.; Ma, X.; Yang, D. Comparison on mechanical properties of heavily phosphorus- and arsenic-doped Czochralski silicon wafers. *AIP Adv.* **2018**, *8*, 045301. [CrossRef]

37. Jlassi, I.; Sdiri, N.; Elhouichet, H.; Ferid, M. Raman and impedance spectroscopy methods of P_2O_5–Li_2O–Al_2O_3 glass system doped with MgO. *J. Alloys Compd.* **2015**, *645*, 125–130. [CrossRef]

38. Reddy, A.S.S.; Jędryka, J.; Oźga, K.; Kumar, V.R.; Purnachand, N.; Kityk, I.; Veeraiah, N. Laser stimulated third harmonic generation studies in ZnO–Ta_2O_5–B_2O_3 glass ceramics entrenched with $Zn_3Ta_2O_8$ crystal phases. *Opt. Mater.* **2018**, *76*, 90–96. [CrossRef]

39. Liu, H.; Chin, T.; Yung, S. FTIR and XPS studies of low-melting PbO–ZnO–P_2O_5 glasses. *Mater. Chem. Phys.* **1997**, *50*, 1–10. [CrossRef]

40. Azmi, S.A.M.; Sahar, M.; Ghoshal, S.; Arifin, R. Modification of structural and physical properties of samarium doped zinc phosphate glasses due to the inclusion of nickel oxide nanoparticles. *J. Non-Cryst. Solids* **2015**, *411*, 53–58. [CrossRef]

41. Shih, P.; Yung, S.; Chin, T. FTIR and XPS studies of P_2O_5–Na_2O–CuO glasses. *J. Non-Cryst. Solids* **1999**, *244*, 211–222. [CrossRef]

42. Resorption, B. Role of Zinc in Bone Formation and Bone resorption. *J. Trace Elem. Exp. Med.* **1998**, *11*, 119–135.

43. Wajda, A.; Sitarz, M. Structural and microstructural studies of zinc-doped glasses from $NaCaPO_4$–SiO_2 system. *J. Non-Cryst. Solids* **2016**, *441*, 66–73. [CrossRef]

44. Kamitakahara, M.; Ohtsuki, C.; Inada, H.; Tanihara, M.; Miyazaki, T. Effect of ZnO addition on bioactive CaO–SiO_2–P_2O_5–CaF_2 glass–ceramics containing apatite and wollastonite. *Acta Biomater.* **2006**, *2*, 467–471. [CrossRef] [PubMed]

45. Müller, L.; Müller, F.A. Preparation of SBF with different HCO_3^- content and its influence on the composition of biomimetic apatites. *Acta Biomater.* **2006**, *2*, 181–189. [CrossRef] [PubMed]

46. Notingher, I.; Boccaccini, A.; Jones, J.R.; Maquet, V.; Hench, L. Application of Raman micro spectroscopy to the characterisation of bioactive materials. *Mater. Charact.* **2002**, *49*, 255–260. [CrossRef]

47. González, P.; Serra, J.; Liste, S.; Chiussi, S.; León, B.; Pérez-Amor, M. Raman spectroscopic study of bioactive silica based glasses. *J. Non-Cryst. Solids* **2003**, *320*, 92–99. [CrossRef]

48. Karakassides, B.M.A.; Saranti, A.; Koutselas, I. Preparation and structural study of binary phosphate glasses with high calcium and/or magnesium content. *J. Non-Cryst. Solids* **2004**, *347*, 69–79. [CrossRef]

49. Chahine, A.; Et-Tabirou, M.; Elbenaissi, M.; Haddad, M.; Pascal, J. Effect of CuO on the structure and properties of $(50-x/2)Na_2O$-$xCuO$-$(50-x/2)P_2O_5$ glasses. *Mater. Chem. Phys.* **2004**, *84*, 341–347. [CrossRef]

50. Ardelean, I.; Rusu, R.; Andronache, C.; Ciobotă, V. Raman study of $xMeO\cdot(100-x)[P_2O_5\cdot Li_2O]$ ($MeO\Rightarrow Fe_2O_3$ or V_2O_5) glass systems. *Mater. Lett.* **2007**, *61*, 3301–3304. [CrossRef]

51. Lucacel, R.C.; Ponta, O.; Simon, V. Short-range structure and in vitro behavior of ZnO–CaO–P_2O_5 bioglasses. *J. Non-Cryst. Solids* **2012**, *358*, 2803–2809. [CrossRef]